Article

Preparation of $Ag_4Bi_2O_5$/MnO_2 Corn/Cob Like Nano Material as a Superior Catalyst for Oxygen Reduction Reaction in Alkaline Solution

Xun Zeng [1], Junqing Pan [1,*] and **Yanzhi Sun [2,*]**

[1] State Key Laboratory of Chemical Resource Engineering, Beijing Engineering Center for Hierarchical Catalysts, Beijing University of Chemical Technology, Beijing 100029, China; 2015201030@mail.buct.edu.cn

[2] National Fundamental Research Laboratory of New Hazardous Chemicals Assessment and Accident Analysis, Beijing University of Chemical Technology, Beijing 100029, China

* Correspondence: jqpan@mail.buct.edu.cn (J.P.); sunyz@mail.buct.edu.cn (Y.S.);
  Tel./Fax: +86-10-6444-8461 (J.P. & Y.S.)

Abstract: $Ag_4Bi_2O_5$/MnO_2 nano-sized material was synthesized by a co-precipitation method in concentrated KOH solution. The morphology characterization indicates that MnO_2 nanoparticles with a size of 20 nm are precipitated on the surface of nano $Ag_4Bi_2O_5$, forming a structure like corn on the cob. The obtained material with 60% Mn offers slightly higher initial potential (0.098 V vs. Hg/HgO) and limiting current density (-5.67 mA cm^{-2}) at a rotating speed of 1600 rpm compared to commercial Pt/C (-0.047 V and -5.35 mA cm^{-2}, respectively). Furthermore, the obtained material exhibits superior long-term durability and stronger methanol tolerance than commercial Pt/C. The remarkable features suggest that the $Ag_4Bi_2O_5$/MnO_2 nano-material is a very promising oxygen reduction reaction catalyst.

1. Introduction

With the rapid consumption of fossil energy, the aggravated emission of carbon dioxide (CO_2) leads to severe environmental issues. In order to reduce the consumption of gasoline, fuel cells, especially Zn-O_2, Li-O_2, and the other metal-air batteries, have been considered as clean power sources, which can directly convert chemical energy into electrical energy with higher energy conversion efficiencies compared with traditional internal combustion engines [1]. However, the scarcity and high cost of platinum or platinum-based catalysts [2–4] commonly used in the cathodic oxygen reduction reaction (ORR) limit the commercialization of fuel cells. Additionally, the platinum (Pt) or platinum-based materials are sensitive to poisoning by methanol [5]. Recently, intensive research has been conducted to develop platinum free catalysts, such as silver (Ag) [6–9], manganese oxide [10–13], and silver/manganese oxide composite [14–16], which are promising catalysts with excellent performance at room temperature for alkaline fuel cells. Manganese oxides are promising catalysts for the oxygen reduction reaction owing to their outstanding activity toward oxygen reduction with the advantages of low cost and abundance [17]. Manganese dioxide (MnO_2) has good catalytic performance towards the oxygen reduction reaction through the integral four electrons mechanism, but its application is limited by the instability of the structure during the discharge process [18]. Silver and its complexes have a good ability to catalyze the oxygen reduction reaction. They were also reported to be more stable than Pt and Pt-based catalysts during long-term operation in alkaline media [7]. Ag and Ag-based materials are insensitive to methanol and can be applied in direct methanol fuel cells (DMFCs) [19]. In addition, Ag and its complexes have a lower price than Pt catalysts. The advantages

of reasonably high electrochemical activity, long-term stability, methanol tolerance, and lower price compared with Pt make Ag and Ag-based composites attractive as catalysts for the oxygen reduction reaction in alkaline media, especially for DMFCs due to the high methanol tolerance of silver. However, the cost of silver and its complexes is still high compared with some other transition metals. It is urgent to develop a facile and green method to synthetize a new catalyst with low cost, relatively excellent electrocatalytic ability for the oxygen reduction reaction, and good stability and methanol tolerance in an alkaline electrolyte.

In this study, a facile method was proposed to prepare nano $Ag_4Bi_2O_5/MnO_2$ material. MnO_2 nano-particles were evenly precipitated on the surface of $Ag_4Bi_2O_5$ nano-rods to form a structure like corn on the cob. The synthesis method has the advantages of low temperature and short synthesis period, and more importantly, MnO_2 can be effectively anchored on the surface of $Ag_4Bi_2O_5$ nano-rods. This material has a comparable catalytic activity to the commercial Pt/C in terms of the oxygen reduction reaction. The catalyst displays superior stability and methanol tolerance compared with the commercial Pt/C. Therefore, nano $Ag_4Bi_2O_5/MnO_2$ material can be an effective catalyst for the oxygen reduction reaction in alkaline solution.

2. Results and Discussion

2.1. Illustration of the Synthesis Process

Figure 1 shows the schematic of the synthesis process of $Ag_4Bi_2O_5/MnO_2$ nano-material. This material was based on $Ag_4Bi_2O_5$ nano-rods with manganese oxide nanoparticles deposited on the surface to form a structure like corn on the cob. The synthesis method was so facile that manipulation at room temperature was enough to effectively precipitate MnO_2 on the surface of the $Ag_4Bi_2O_5$ rods. This structure is conducive to the synergistic effect of the three metals (Ag, Bi, and Mn) and the adsorption of O_2 on the surface of the catalyst as well as the disconnection of the O-O bonds. The nanostructure can effectively reduce the size of the catalyst and increase the specific surface area so that more catalytic activity sites are exposed and the oxygen reduction process can be catalyzed in a stable and efficient way [20]. Therefore, $Ag_4Bi_2O_5/MnO_2$ can be considered as a promising catalyst for the oxygen reduction reaction.

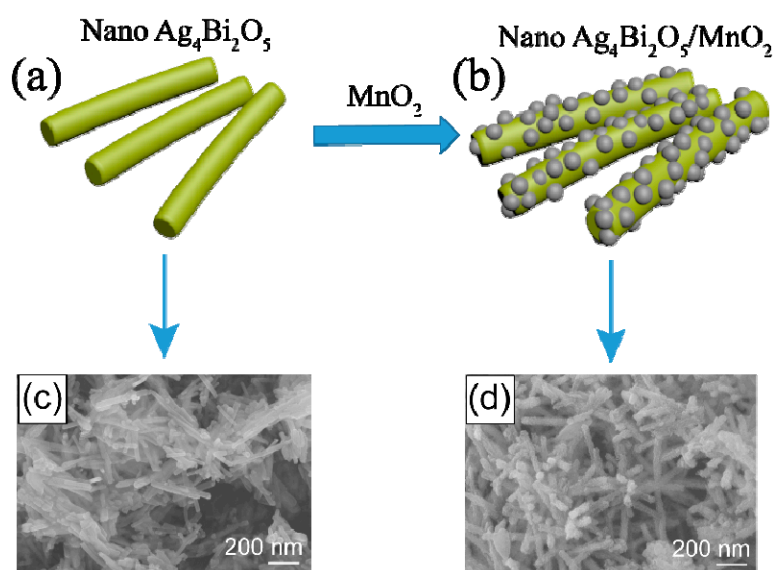**Figure 1.** Schematic drawing of the synthesis process of nano $Ag_4Bi_2O_5/MnO_2$ material. (**a**) diagram of nano $Ag_4Bi_2O_5$; (**b**) diagram of nano $Ag_4Bi_2O_5/MnO_2$; (**c**) SEM image of nano $Ag_4Bi_2O_5$; (**d**) SEM image of nano $Ag_4Bi_2O_5$.

2.2. Structural and Morphological Characterizations

As is clearly illustrated in Figure 2, when $Ag_4Bi_2O_5$ is added to manganese dioxide, the X-ray powder diffraction (XRD) patterns of the samples (0–60% Mn) still have the typical characteristic peaks of $Ag_4Bi_2O_5$. From the XRD patterns, it was found that the samples were typical at $2\theta = 26.37°$, $31.25°$, $31.85°$, $37.76°$ and $56.19°$ corresponding to (112), (411), (312), (600), and (332) of the $Ag_4Bi_2O_5$, respectively, according to the standard JCPDS 87-0866 of $Ag_4Bi_2O_5$. The peaks of $Ag_4Bi_2O_5/MnO_2$ are broad, indicating that the incorporation of Mn affects the crystalline structure of $Ag_4Bi_2O_5$. There are no typical peaks of MnO_2 because the MnO_2 is amorphous.
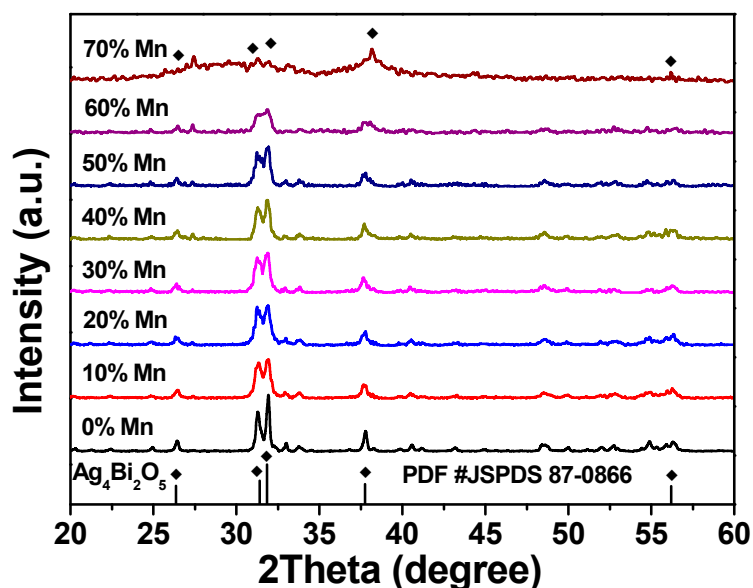

Figure 2. X-ray powder diffraction (XRD) patterns of $Ag_4Bi_2O_5/MnO_2$ with different ratios of manganese dioxide contents from 0% to 70%.

Scanning electron microscopy (SEM) images in Figure 3 of the $Ag_4Bi_2O_5/MnO_2$ samples show the morphological and structural information. It can be seen in Figure 3a that nano $Ag_4Bi_2O_5$ are smooth rods with length and width of 200 nm and 30 nm, respectively. When the amount of manganese dioxide is 10–60%, there are some nano particles on the rod-like $Ag_4Bi_2O_5$, and the length and width is still about 200 nm and 30 nm, respectively. With the increase of the ratio of manganese dioxide, there are more nano particles on the nano rods. The structure is beneficial to the synergistic effect of Ag, Bi, and Mn in catalyzing the oxygen reduction reaction. The nanostructure can reduce the size of the catalyst and more catalytic activity sites are exposed so that the oxygen reduction process can be catalyzed in a stable and efficient manner. When the amount of manganese oxide is 70%, the material particles become larger, and the length and width are about 400 nm and 100 nm, respectively.

The results of transmission electron microscope (TEM) and high-resolution transmission electron microscopy (HRTEM) are shown in Figure 4. It can be seen from Figure 4a that MnO_2 is distributed on the surface of rod-like $Ag_4Bi_2O_5$. The HRTEM image of $Ag_4Bi_2O_5$ with 60% Mn was used to further demonstrate the detailed structural features of the material. The distances between the lattice planes are 0.333 nm and 0.417 nm corresponding to the planes of $Ag_4Bi_2O_5$ (112) and $Ag_4Bi_2O_5$ (301), respectively (Figure 4b). There are no planes of MnO_2 because it is amorphous. This result is consistent with the result of XRD.
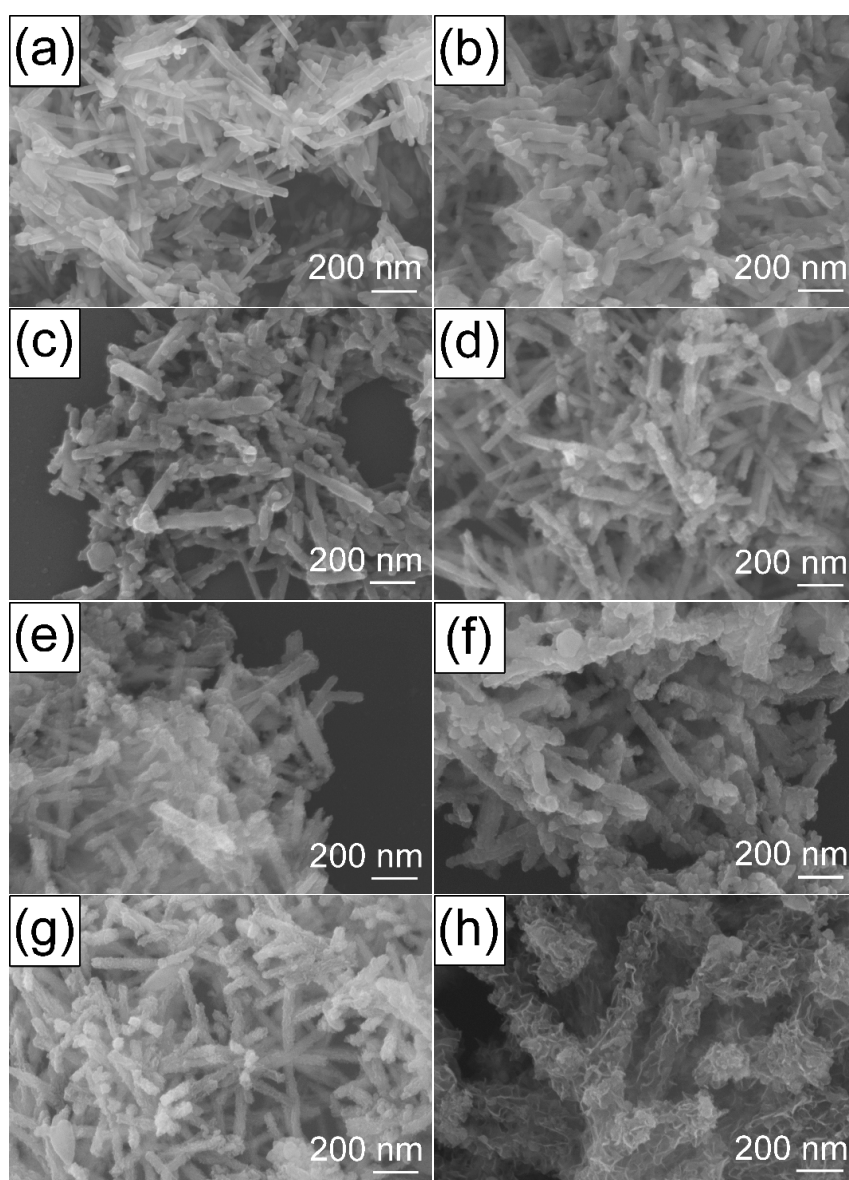
Figure 3. Scanning electron microscopy (SEM) images of $Ag_4Bi_2O_5/MnO_2$ with different ratios of manganese dioxides contents, (**a**) 0%; (**b**) 10%; (**c**) 20%; (**d**) 30%; (**e**) 40%; (**f**) 50%; (**g**) 60%; and (**h**) 70% Mn.

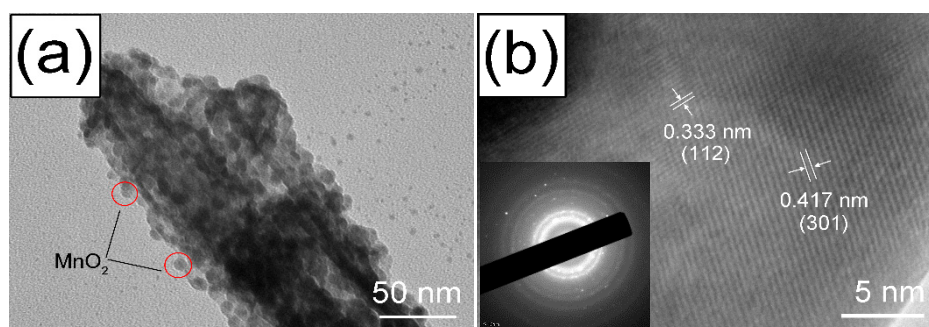**Figure 4.** (**a**) Transmission electron microscopy (TEM) image of $Ag_4Bi_2O_5$ with 60% Mn, (**b**) high-resolution transmission electron microscopy (HRTEM) image of $Ag_4Bi_2O_5$ with 60% Mn.

In order to explore the elemental distribution of $Ag_4Bi_2O_5$ with 60% Mn, mapping analysis of $Ag_4Bi_2O_5$ with 60% Mn was performed as in Figure 5. It can be seen that the four elements of O, Ag, Bi, and Mn are evenly distributed. Energy dispersive spectrometer (EDS) analysis was also performed to obtain the chemical composition shown in Figure 6. It is proved that the presence of O, Ag, Bi, and Mn elements and the successful synthesis of $Ag_4Bi_2O_5$ with 60% Mn. The atomic ratios of Ag, Bi, and Mn are 15.56%, 7.57%, and 6.15%, respectively. The ratio of Bi and Mn is 1.23, which is close to the theoretical ratio of 1.33. The atomic ratio of Ag:Bi conforms to the atomic ratio 2:1 in the $Ag_4Bi_2O_5$.

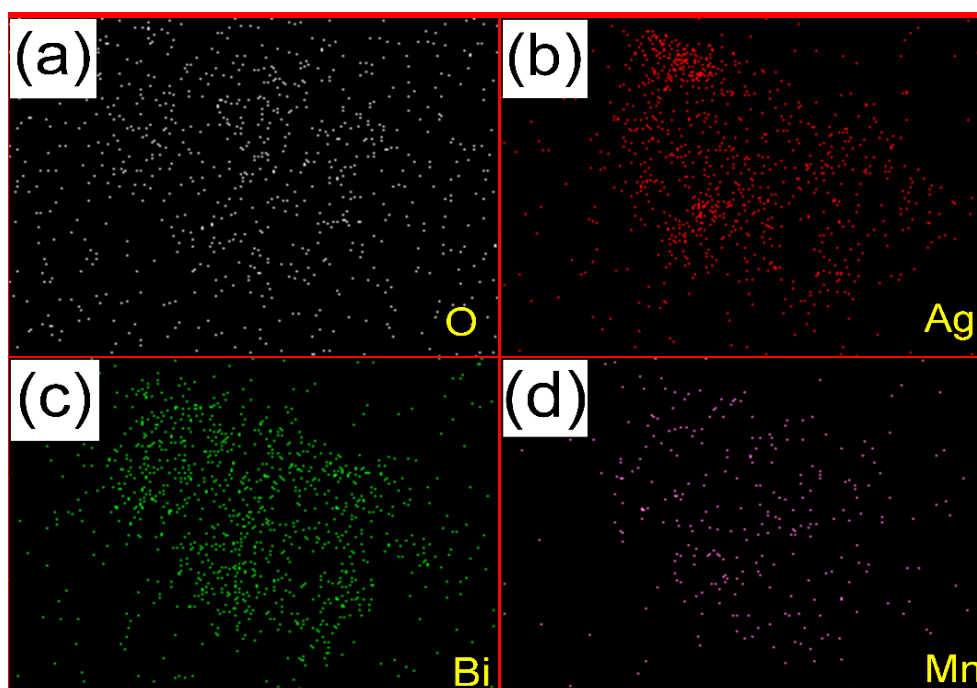**Figure 5.** Elemental mapping images of $Ag_4Bi_2O_5$ with 60% Mn (**a**) O element, (**b**) Ag element, (**c**) Bi element, (**d**) Mn element.

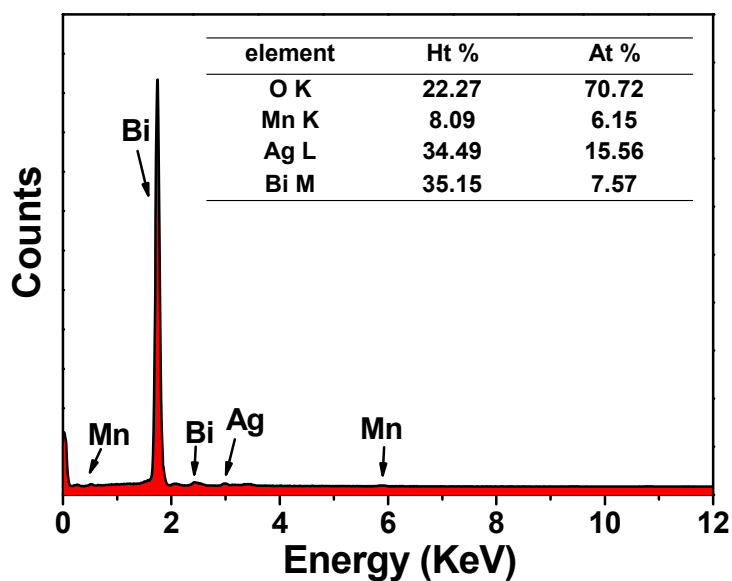| element	Ht %	At %
O K	22.27	70.72
Mn K	8.09	6.15
Ag L	34.49	15.56
Bi M	35.15	7.57

Figure 6. Energy dispersive spectrometry (EDS) analysis of $Ag_4Bi_2O_5$ with 60% Mn.

To investigate the elemental compositions and the valences of the elements in the as prepared $Ag_4Bi_2O_5$ with 60% Mn composite, X-ray photoelectron spectroscopy (XPS) was employed. The results are shown in Figure 7. Figure 7a shows the XPS survey spectra. Figure 7b–d shows the high resolution spectra of Ag 3d, Bi 4f, and Mn 2p of $Ag_4Bi_2O_5/MnO_2$, respectively. In Figure 7b, it can be seen that the peaks at 368.2 eV and 374.2 eV are Ag $3d_{5/2}$ and Ag $3d_{3/2}$, respectively. These two peaks show that the valence state of Ag is +1 [21]. The two peaks at 158.8 eV and 163.9 eV in Figure 7c correspond to Bi $3f_{7/2}$ and Bi $3f_{5/2}$, respectively, proving the presence of Bi of +3 [21]. Figure 7d shows the XPS spectra of the 2p orbital of the Mn element in $Ag_4Bi_2O_5/MnO_2$. The two peaks at 642 eV and 653.7 eV correspond to Mn $2p_{3/2}$ and Mn $2p_{1/2}$ of Mn^{4+}, respectively, which indicates that the valence state of the whole material is dominated by MnO_2 which is on the surface [22].
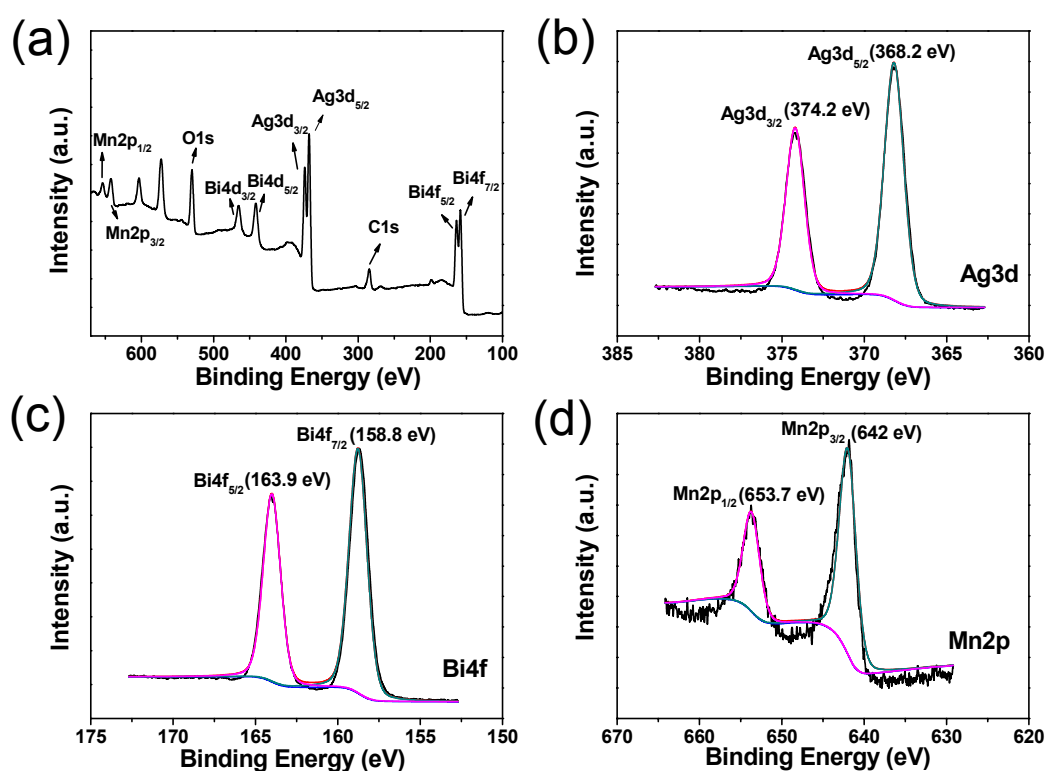

Figure 7. X-ray photoelectron spectroscopy (XPS) spectra of (**a**) $Ag_4Bi_2O_5$ with 60% Mn, (**b**) XPS spectra of Ag 3d, (**c**) XPS spectra of Bi 4f, (**d**) XPS spectra of Mn 2p.

2.3. Electrocatalytic Performance

To provide an insight into the activity of ORR on the $Ag_4Bi_2O_5/MnO_2$ material, linear sweep voltammetry (LSV) plots were tested by a rotating disk electrode (RDE) at a speed of 1600 rpm in O_2-saturated 0.1 mol L^{-1} KOH solution at a scanning rate of 5 mV s^{-1}. MnO_2, $Ag_4Bi_2O_5$, and commercial Pt/C was also investigated under the same conditions. The starting potential is the potential at the limiting current density of 0.1 mA cm^{-2} [23]. It is shown in Figure 8a and Table 1 that the initial potential (v_o), half-wave potential ($v_{1/2}$), and limiting current density (j) of $Ag_4Bi_2O_5$ is -0.09 V, -0.227 V, and -2.06 mA cm^{-2}, respectively. With the increase of content of MnO_2, the materials have a better ability to catalyze ORR due to the increase of the synergistic effects of Ag, Bi, and Mn. The initial potential, half-wave potential and limiting current density of $Ag_4Bi_2O_5$ with 60% Mn are 0.098 V, -0.047 V, and -5.67 mA cm^{-2}, respectively, which shows that this has the best ability to catalyze the oxygen reduction reaction compared to any other ratio of $Ag_4Bi_2O_5/MnO_2$. In addition, $Ag_4Bi_2O_5$ with 70% Mn is poor for catalyzing ORR although MnO_2 is increased. This result is due to the particles of the material becoming larger, leading to fewer catalytic activity sites thus reducing the

activity for catalyzing the oxygen reduction reaction compared with 10–60% Mn. Figure 8b shows the RDE curves of $Ag_4Bi_2O_5$ with 60% Mn at different rotation speeds (400–2500 rpm). Figure 8c shows the Koutecky-Levich (K-L) plots which describe the relation between the inverse real current density (j^{-1}) and the inverse of the square root of the rotating rate ($\omega^{-1/2}$) [22]. The good linearity of the K-L plots reveals that the kinetics of the ORR is first-order with respect to the concentration of dissolved oxygen and similar electron transfer numbers at different potentials [24].

$$\frac{1}{i} = \frac{1}{i_k} + \frac{1}{i_d}$$

$$i_k = nfkC_0$$

$$i_d = 0.62nFD_0^{2/3}v^{-1/6}C_0\omega^{1/2}$$

Here, n is number of electrons involved in the reaction, F is the Faraday constant (96,500 C mol^{-1}), D_0 is the diffusion coefficient of oxygen in the electrolyte (0.1 mol L^{-1} KOH solution) (1.93 × 10^{-5} cm^2 s^{-1}), v is the viscosity coefficient of the solution (0.1 cm^2 s^{-1}), C_0 is the concentration of O_2 in 0.1 mol L^{-1} KOH solution (1.26 × 10^{-3} mol L^{-1}), ω is the speed of the disc (rad s^{-1}) [25,26]. As calculated from Figure 8d in the potential range from −0.25 V to −0.35 V, the average number of transferring electrons of ORR on the $Ag_4Bi_2O_5$ with 60% Mn is about 3.9, indicating that the ORR catalyzed by the $Ag_4Bi_2O_5$ with 60% Mn follows the most efficient four-electron mechanism.
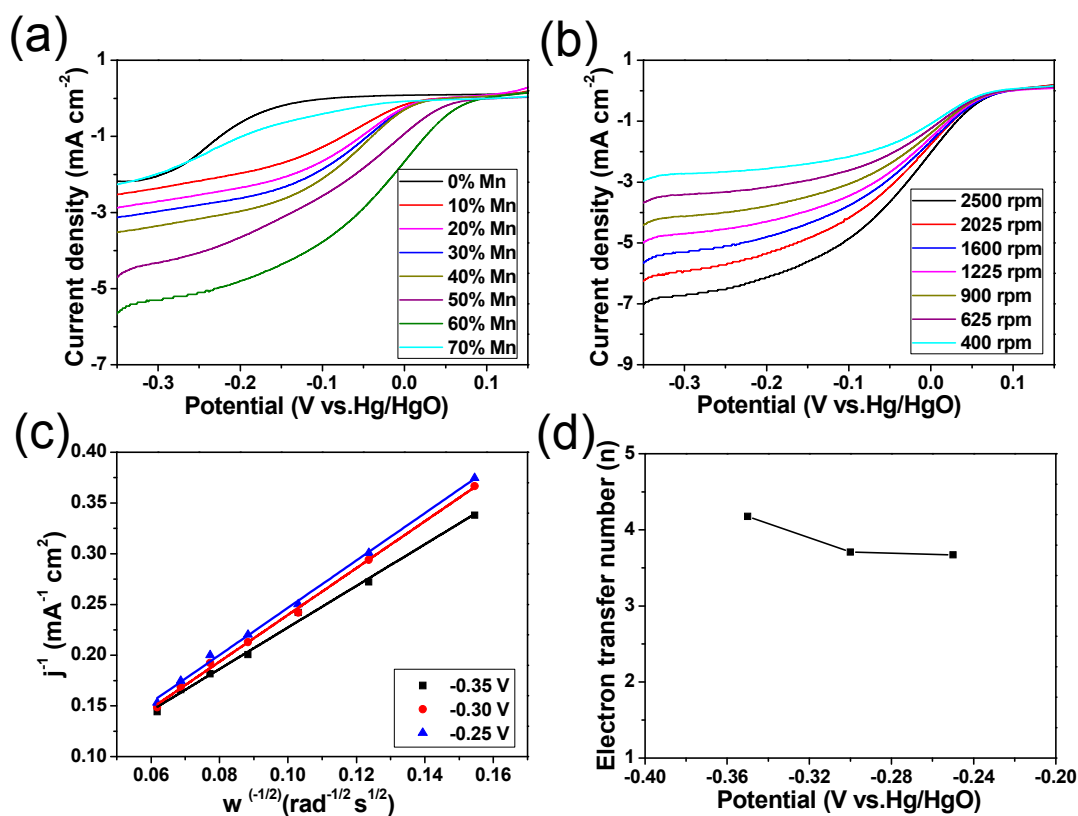
Figure 8. In 0.1 mol L^{-1} KOH solution, (**a**) linear sweep voltammetry (LSV) curves of $Ag_4Bi_2O_5$ with different ratios of manganese dioxides (0% Mn to 70% Mn) with O_2 saturation at a potential scanning rate of 5 mV s^{-1} and a rotation speed of 1600 rpm, (**b**) LSV curves of $Ag_4Bi_2O_5$ with 60% Mn at different rotation speeds (400–2500 rpm) at scanning rate of 5 mV s^{-1}, (**c**) Koutecky-Levich curves of $Ag_4Bi_2O_5$ with 60% Mn at different potentials, (**d**) Number of transferring electrons at the corresponding potentials.

Table 1. Initial potential (v_o), half-wave potential ($v_{1/2}$) and limiting current density (j) of commercial Pt/C and $Ag_4Bi_2O_5$ with different contents of MnO_2.

Parameter	v_o (V vs. Hg/HgO)	$v_{1/2}$ (V vs. Hg/HgO)	J (mA cm^{-2})
0% Mn	−0.09	−0.227	−2.06
10% Mn	0.042	−0.123	−3.00
20% Mn	0.046	−0.099	−3.086
30% Mn	0.052	−0.090	−3.23
40% Mn	0.052	−0.078	−3.52
50% Mn	0.111	−0.084	−4.70
60% Mn	0.098	−0.047	−5.67
70% Mn	0.107	−0.219	−2.41
100% Mn	−0.014	−0.203	−2.19
Pt/C	0.179	−0.014	−5.09

To further elucidate the electrochemical performance of the $Ag_4Bi_2O_5/MnO_2$ materials, the electrochemically active surface area (ECSA) can be evaluated through a simple cyclic voltammetry (CV) measurement as in Figure S1 [27]. The calculated electrochemically effective double-layer capacitances (C_{dl}) shown in Figure S2 are 0.92, 1.39, 1.51, 2.07, 2.47, 3.78, 5.02, and 1.34 mF cm^{-2} for 0%, 10%, 20%, 30%, 40%, 50%, 60%, and 70% Mn, respectively. This result indicates that $Ag_4Bi_2O_5$ with 60% Mn can expose most electrochemically active sites during the ORR process.

It is inferred that the obtained $Ag_4Bi_2O_5$ with 60% Mn catalyst offers a larger enhanced electrocatalytic activity than $Ag_4Bi_2O_5$ and MnO_2 in Figure 9a,b. The initial potential (v_o), half-wave potential ($v_{1/2}$) and limiting current density (j) of $Ag_4Bi_2O_5$ with 60% Mn are 0.098 V, −0.047 V, and −5.67 mA cm^{-2}, respectively. Compared with commercial Pt/C, the initial potential and half-wave potential of $Ag_4Bi_2O_5$ with 60% Mn are 0.005 V more positive (Pt/C, 0.093 V) and 0.017 V more negative (Pt/C, −0.03 V), respectively, and the limiting current density is slightly higher than Pt/C, showing the performance of $Ag_4Bi_2O_5$ with 60% Mn toward oxygen reduction reaction is close to Pt/C in potential and slightly superior in current density. Previous papers showed that the doping of Bi_2O_3 and $NaBiO_3$ into MnO_2 would enhance the durability during the discharge process [21,28,29]. The new material of $Ag_4Bi_2O_5/MnO_2$ displays two beneficial functions for both couples of Mn-Bi and Ag-Mn. The former plays an important role of strong support of the structure of MnO_2, which will greatly enhance the durability of the catalyst, and the latter offers remarkable catalytic performance compared to the single Ag or Mn compound. The electrocatalytic activity of $Ag_4Bi_2O_5$ with 60% Mn towards ORR was examined by CV in 0.1 mol L^{-1} KOH solution saturated with O_2 and Ar, respectively, at a sweep rate of 50 mV s^{-1}. The oxygen reduction peak of $Ag_4Bi_2O_5$ with 60% Mn is at −0.09 V and the peak current density is 1.53 mA cm^{-2} in electrolyte solution saturated with O_2, as shown in Figure 9c,d shows the Tafel of $Ag_4Bi_2O_5$ with 60% Mn and commercial Pt/C. The Tafel slope of the $Ag_4Bi_2O_5$ with 60% Mn and commercial Pt/C are 73 and 68 mV dec^{-1}, respectively. The low ORR Tafel slope of $Ag_4Bi_2O_5$ with 60% Mn implies a transition from Langmuirian adsorption to Temkin adsorption of adsorbed O/OH groups [30]. Therefore, the electrochemical catalyst activation of $Ag_4Bi_2O_5$ with 60% Mn is close to that of Pt/C [15]. The long-term stability was assessed in O_2-saturated 0.1 mol L^{-1} KOH solution by chrono-amperometry. $Ag_4Bi_2O_5/MnO_2$ has a small decay of −13% in ORR activity after 10,800 s, while Pt/C has an attenuation of 18% shown in Figure 9e. In addition, the current density of the Pt/C shows a much sharper decrease when methanol is introduced in the electrolyte (Figure 9f), while the current density of $Ag_4Bi_2O_5/MnO_2$ only exhibits a small decrease under the same conditions. This means that $Ag_4Bi_2O_5/MnO_2$ displays superior stability and methanol tolerance compared to the commercial Pt/C.

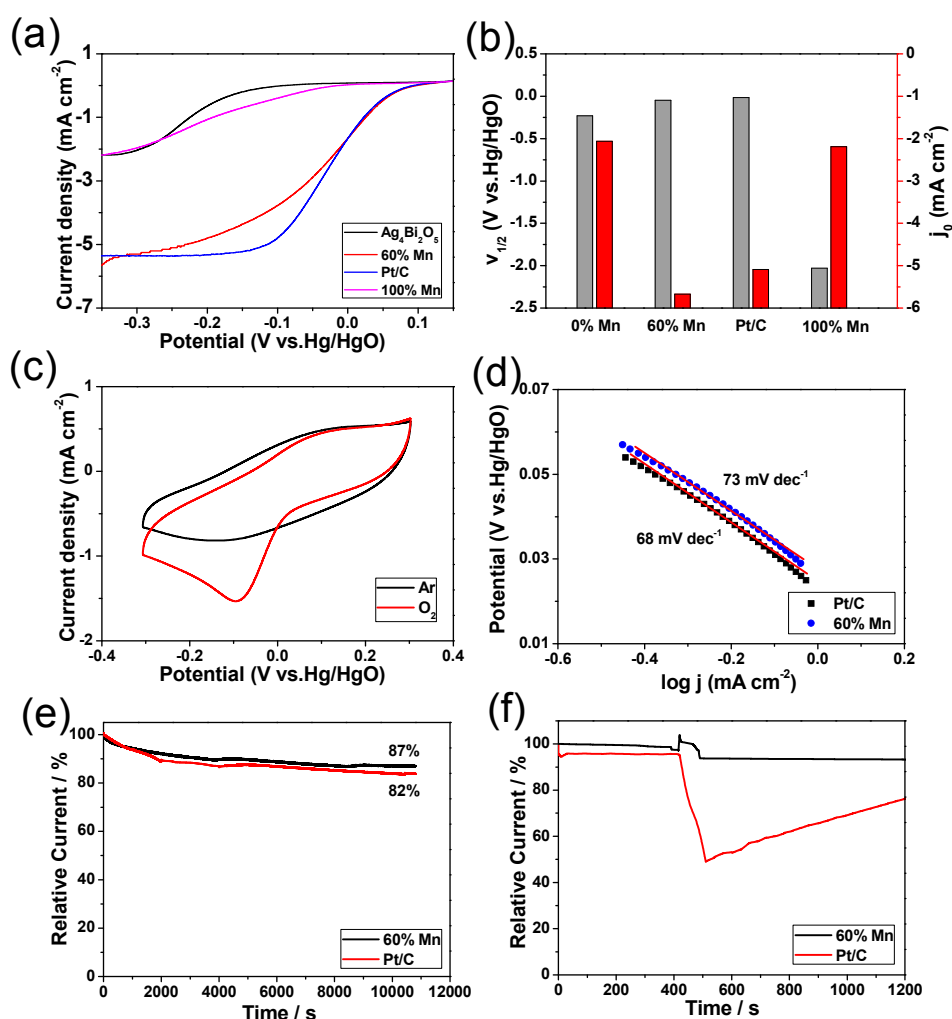**Figure 9.** (**a**) LSV curves of $Ag_4Bi_2O_5$ with 60% Mn, Pt/C and MnO_2 by rotating disk electrode (RDE) in KOH solution with O_2 saturation at a speed of 5 mV s^{-1} and a rotation speed of 1600 rpm, (**b**) comparison between commercial Pt/C and $Ag_4Bi_2O_5$ with 0% Mn, 60% Mn, 100% Mn, at half-wave potential ($v_{1/2}$) and current density (j), (**c**) cyclic voltammetry (CV) curves of $Ag_4Bi_2O_5$ with 60% Mn at a scan rate of 50 mV s^{-1} with Ar and O_2 saturation, respectively, (**d**) Tafel curves of $Ag_4Bi_2O_5$ with 60% Mn and commercial Pt/C, (**e**) i-t chrono-amperometric curves of $Ag_4Bi_2O_5$ with 60% Mn and Pt/C at -0.26 V with O_2 saturation at a rotation speed of 1600 rpm, (**f**) methanol tolerance of $Ag_4Bi_2O_5$ with 60% Mn and commercial Pt/C by chronoamperometric response with O_2 saturation for 1200 s and adding 3.0 mol L^{-1} CH_3OH at about the 420th second.

Table 2. Comparison of oxygen reduction reaction (ORR) catalytic activities between $Ag_4Bi_2O_5$ with 60% Mn and the other relevant catalysts.

Catalyst	E_0 (V vs. Hg/HgO)	$E_{1/2}$ (V vs. Hg/HgO)	Currents (mA cm^{-2})	Stability	Reference
$Ag_4Bi_2O_5$ with 60% Mn	0.098	-0.047	5.67	88% (10,800 s)	This work
Mn_3O_4/NrGO	-0.1	-0.2	4.4	63% (21,600 s)	[10]
$Ag@MnFe_2O_4$/C	-0.08	-0.171	4.8	88.7% (15,000 s)	[31]
50% $Ag-MnO_2$/C	-0.036	-0.216	5.5	91% (50,000 s)	[32]
SC-PMO	-0.037	-0.237	5.0	82% (16,000 s)	[33]
C_{PANI}/Mn_2O_3	0.108	-0.082	5.61	91.1% (80,000 s)	[34]
rGO/MnO_2/Ag	0.034	-0.126	3.4	94% (10,000 s)	[35]
$Ag-PBMO_5$	0.054	-0.056	5.0	91% (50,000 s)	[36]
Ag/$Cu_{37}Pd_{63}$	0.05	-0.04	2.96	77.6% (48,000 s)	[37]

Recently, several papers all from prestigious journals have reported several catalysts with good ORR performance. The catalytic properties of these materials and the as-prepared $Ag_4Bi_2O_5$ with 60% Mn in this study are compared in Table 2. Among all the listed catalysts, the $Ag_4Bi_2O_5$ with 60% Mn shows the most efficient ORR performance with positive initial potential and half-wave potential, high limiting current density, and excellent long-term stability [33–37]. The comparison shows that $Ag_4Bi_2O_5$ with 60% Mn is a highly efficient catalyst for ORR.

3. Experimental

3.1. Reagents

All the chemicals were analytical grade and used as received without further purification. Ag_2O, Bi_2O_3, $Mn(NO_3)_2$, HNO_3, and isopropanol were commercially available from Tianjin Fuchen Industry Co. Ltd. (Tianjin, China). KOH was purchased from Chengdu Huarong Chemical Reagent Co. Ltd. (Chengdu, China). Commercial Pt/C (20 wt%, Hispec 3000) was obtained from Johnson Matthey Company (London, UK). Conductive graphite (Timcal-ks6) was available Timical Company (Changzhou, China). Nafion solution (5 wt%, D520) was from DuPont (Wilmington, NC, USA).

3.2. Synthesis and Physical Characterizations

An amount of 100 mL 6.5 mol L^{-1} KOH was employed as basic solution, marked as solution A. Then 1.16 g Ag_2O and 1.17 g Bi_2O_3 were dissolved in 50 mL 1 mol L^{-1} HNO_3, and the mixture solution was marked as solution B. The solution B was added into the solution A at a rate of 3 mL min^{-1}. After complete reaction of the solutions A and B, the resulting solution was aged for 1 h and marked as solution C.

Amounts of 0 g, 0.1 g, 0.22 g, 0.38 g, 0.60 g, 0.89 g, 1.34 g, and 2.09 g of 50% $Mn(NO_3)_2$ solutions were dissolved in deionized water to prepare portions of 20 mL solutions, respectively. These eight $Mn(NO_3)_2$ solutions were dripped into the above solution C at a rate of 3 mL min^{-1}, respectively. After crystallization for 2 h, the samples were washed with deionized water until pH = 7, and then dried in vacuum at 303.15 K for 8 h. The materials were named 0% Mn, 10% Mn, 20% Mn, 30% Mn, 40% Mn, 50% Mn, 60% Mn, and 70% Mn by ratio of moles.

All the preparation was conducted under conditions of room temperature and a strong agitation at 2000 rpm.

3.3. Physicochemical Characterization

The phase structures of samples were analyzed by a Rigaku D/max2500VB2+/PC X-ray diffractometer (XRD) with a Cu Kα anticathode (40 kV, 200 mA) (Rigaku Corporation, Tokyo, Japan). The morphology and surface structure of $Ag_4Bi_2O_5/MnO_2$ were investigated by using scanning electron microscopy (SEM, ZEISS, SUPRA 55, Carl Zeiss AG, Oberkochen, Germany), transmission electron microscope (TEM, Hitachi, H-7700, Hitachi Company, Tokyo, Japan) and high resolution transmission electron microscope (HR-TEM, JEOL JEM-2100F, JEOL Company, Tokyo, Japan). The elemental mapping and energy dispersive spectrometer (EDS) was carried out on an X-ray energy instrument (LINK-ISIS300, Oxford, UK). The valences of elements were analyzed by using an X-ray photoelectron spectrometer (XPS, Thermo VG Scientic ESCALAB 250, Thermo Fisher Scientific, Waltham, MA, USA).

3.4. Electrochemical Measurements

The electrochemical performance of the $Ag_4Bi_2O_5/MnO_2$ samples was tested on a rotating disk electrode with a diameter of 5 mm (RDE, AFMRSCE, Pine Instrument, Grove, PA, USA) at rotation speeds of 400–2500 rpm and a potential sweeping rate of 5 mV s^{-1} by linear sweep voltammetry (LSV). A Hg/HgO electrode was used as the reference electrode, and a platinum wire as the auxiliary

electrode. The working electrode was prepared as follows: 8 mg catalyst and 4 mg conductive graphite were dispersed ultrasonically for 30 min in a mixture of 55 μL Nafion solution, 430 μL isopropanol and 650 μL deionized water to form catalyst ink. Then 5.6 μL of the ink was spread on the glassy carbon electrode (GCE) and dried at room temperature. The working electrode was loaded with a catalyst amount of 0.2 mg cm^{-2}. Cyclic voltammetry (CV) of $Ag_4Bi_2O_5/MnO_2$ was conducted using an electrochemical workstation (CHI 760d, Chenhua Instruments, Shanghai, China). The potential range of the CV was between -0.3 V and 0.3 V (V vs. Hg/HgO). The electrochemical tests of LSV, CV, and Tafel were performed in 0.1 mol L^{-1} KOH solution saturated with oxygen (O_2) or argon (Ar) gas. The i-t chronoamperometric was tested at -0.26 V with O_2 saturation for 10,800 s. The methanol tolerance test was performed in 0.1 mol L^{-1} KOH solution saturated with O_2 for 1200 s and 3.0 mol L^{-1} CH_3OH was added at about the 420th second. The results were shown by chronoamperometry curves. For comparison, $Ag_4Bi_2O_5$, and MnO_2 were also tested by the same procedure.

4. Conclusions

$Ag_4Bi_2O_5/MnO_2$ nano-material was successfully synthesized by a co-precipitation method. The MnO_2 nano particles were distributed on the surface of rod-like $Ag_4Bi_2O_5$ crystals to form a structure like corn on the cob. Compared with a commercial Pt/C catalyst, the $Ag_4Bi_2O_5$ with 60% Mn nano-material has an equivalent ORR activity in alkaline media, but a better stability and methanol tolerance. The excellent electrochemical activity of $Ag_4Bi_2O_5/MnO_2$ might benefit from the synergistic effects of Ag, Bi, and Mn as well as more active sites. The synergistic effects of the Ag-Mn elements remarkably enhanced the catalytic activity. The Bi-Mn elements and the corn-cob like structure of $Ag_4Bi_2O_5/MnO_2$ are propitious to strengthen the stability of the catalyst. More active sites contribute to the adsorption of O_2 on the catalyst surface and the breakage of O-O bonds. In alkaline conditions, the catalyst can catalyze the oxygen reduction reaction through the four-electron mechanism. Therefore, nano $Ag_4Bi_2O_5/MnO_2$ has proved to be a very promising oxygen reduction catalyst under alkaline conditions.

Supplementary Materials: The following are available online at www.mdpi.com/2073-4344/7/12/379/s1, Figure S1: CV curves of $Ag_4Bi_2O_5$ with different content of MnO_2, (a) 0%; (b) 10%; (c) 20%; (d) 30%; (e) 40%; (f) 50%; (g) 60%; (h) 70%, Figure S2: Extraction of the C_{dl} for $Ag_4Bi_2O_5/MnO_2$ with different ratios of manganese dioxides.

Author Contributions: Junqing Pan proposed the concept, and supervised the research work at BUCT. Xun Zeng, Junqing Pan, and Yanzhi Sun designed the experiments; Xun Zeng performed the experiments. All authors analyzed the data and wrote the paper.

Conflicts of Interest: The authors declare no conflict of interest.

References

1. Steele, B.C.; Heinzel, A. Materials for fuel-cell technologies. *Nature* **2001**, *414*, 345–352. [CrossRef] [PubMed]
2. Chauhan, S.; Mori, T.; Masuda, T.; Ueda, S.; Richards, G.J.; Hill, J.P.; Ariga, K.; Isaka, N.; Auchterlonie, G.; Drennan, J. Design of Low Pt Concentration Electrocatalyst Surfaces with High Oxygen Reduction Reaction Activity Promoted by Formation of a Heterogeneous Interface between Pt and CeO$_x$ Nanowire. *ACS Appl. Mater. Interfaces* **2016**, *8*, 9059–9070. [CrossRef] [PubMed]
3. Escuderoescribano, M.; Malacrida, P.; Hansen, M.H.; Vejhansen, U.G.; Velazquezpalenzuela, A.; Tripkovic, V.; Schiotz, J.; Rossmeisl, J.; Stephens, I.E.; Chorkendorff, I. Tuning the activity of Pt alloy electrocatalysts by means of the lanthanide contraction. *Science* **2016**, *352*, 73–76. [CrossRef] [PubMed]
4. Gan, L.; Heggen, M.; Cui, C.; Strasser, P. Thermal Facet Healing of Concave Octahedral Pt-Ni Nanoparticles Imaged in Situ at the Atomic Scale: Implications for the Rational Synthesis of Durable High-Performance ORR Electrocatalysts. *ACS Catal.* **2016**, *6*, 692–695. [CrossRef]
5. Gautam, R.K.; Bhattacharjee, H.; Venkata Mohan, S.; Verma, A. Nitrogen doped graphene supported α-MnO$_2$ nanorods for efficient ORR in a microbial fuel cell. *RSC Adv.* **2016**, *6*, 110091–110101. [CrossRef]

6. Lu, Y.; Chen, W. Size effect of silver nanoclusters on their catalytic activity for oxygen electro-reduction. *J. Power Sources* **2012**, *197*, 107–110. [CrossRef]

7. Liu, M.; Chen, W. Green synthesis of silver nanoclusters supported on carbon nanodots: Enhanced photoluminescence and high catalytic activity for oxygen reduction reaction. *Nanoscale* **2013**, *5*, 12558–12564. [CrossRef] [PubMed]

8. Sekol, R.C.; Li, X.; Cohen, P.; Doubek, G.; Carmo, M.; Taylor, A.D. Silver palladium core-shell electrocatalyst supported on MWNTs for ORR in alkaline media. *Appl. Catal. B Environ.* **2013**, *138*, 285–293. [CrossRef]

9. Wang, Q.; Cui, X.; Guan, W.; Zhang, L.; Fan, X.; Shi, Z.; Zheng, W. Shape-dependent catalytic activity of oxygen reduction reaction (ORR) on silver nanodecahedra and nanocubes. *J. Power Sources* **2014**, *269*, 152–157. [CrossRef]

10. Bikkarolla, S.K.; Yu, F.; Zhou, W.; Joseph, P.; Cumpson, P.; Papakonstantinou, P. A three-dimensional Mn_3O_4 network supported on a nitrogenated graphene electrocatalyst for efficient oxygen reduction reaction in alkaline media. *J. Mater. Chem. A* **2014**, *2*, 14493. [CrossRef]

11. Meng, Y.; Song, W.; Huang, H.; Ren, Z.; Chen, S.Y.; Suib, S.L. Structure-property relationship of bifunctional MnO_2 nanostructures: Highly efficient, ultra-stable electrochemical water oxidation and oxygen reduction reaction catalysts identified in alkaline media. *J. Am. Chem. Soc.* **2014**, *136*, 11452–11464. [CrossRef] [PubMed]

12. Wei, C.; Yu, L.; Cui, C.; Lin, J.; Wei, C.; Mathews, N.; Huo, F.; Sritharan, T.; Xu, Z. Ultrathin MnO_2 nanoflakes as efficient catalysts for oxygen reduction reaction. *Chem. Commun.* **2014**, *50*, 7885–7888. [CrossRef] [PubMed]

13. Du, J.; Chen, C.; Cheng, F.; Chen, J. Rapid Synthesis and Efficient Electrocatalytic Oxygen Reduction/Evolution Reaction of $CoMn_2O_4$ Nanodots Supported on Graphene. *Inorg. Chem.* **2015**, *54*, 5467–5474. [CrossRef] [PubMed]

14. Liu, J.; Liu, J.; Song, W.; Wang, F.; Song, Y. The role of electronic interaction in the use of Ag and Mn_3O_4 hybrid nanocrystals covalently coupled with carbon as advanced oxygen reduction electrocatalysts. *J. Mater. Chem. A* **2014**, *2*, 17477–17488. [CrossRef]

15. Liu, S.; Qin, X. Preparation of a Ag-MnO_2/graphene composite for the oxygen reduction reaction in alkaline solution. *RSC Adv.* **2015**, *5*, 15627–15633. [CrossRef]

16. Park, S.A.; Lim, H.; Kim, Y.T. Enhanced Oxygen Reduction Reaction Activity Due to Electronic Effects between Ag and Mn_3O_4 in Alkaline Media. *ACS Catal.* **2015**, *5*, 3995–4002. [CrossRef]

17. Ryabova, A.S.; Napolskiy, F.S.; Poux, T.; Istomin, S.Y.; Bonnefont, A.; Antipin, D.M.; Baranchikov, A.Y.; Levin, E.E.; Abakumov, A.M.; Kéranguéven, G.; et al. Rationalizing the Influence of the Mn(IV)/Mn(III) Red-Ox Transition on the Electrocatalytic Activity of Manganese Oxides in the Oxygen Reduction Reaction. *Electrochim. Acta* **2016**, *187*, 161–172. [CrossRef]

18. Li, L.; Hu, Z.A.; An, N.; Yang, Y.Y.; Li, Z.M.; Wu, H.Y. Facile Synthesis of MnO_2/CNTs Composite for Supercapacitor Electrodes with Long Cycle Stability. *J. Phys. Chem. C* **2014**, *118*, 22865–22872. [CrossRef]

19. Tang, Q.; Jiang, L.; Qi, J.; Jiang, Q.; Wang, S.; Sun, G. One step synthesis of carbon-supported Ag/Mn_yO_x composites for oxygen reduction reaction in alkaline media. *Appl. Catal. B Environ.* **2011**, *104*, 337–345. [CrossRef]

20. Cheng, F.; Su, Y.; Liang, J.; Tao, Z.; Chen, J. MnO_2-Based Nanostructures as Catalysts for Electrochemical Oxygen Reduction in Alkaline Media. *Chem. Mater.* **2014**, *22*, 898–905. [CrossRef]

21. Sun, Y.; Yang, M.; Pan, J.; Wang, P.; Li, W.; Wan, P. Manganese dioxide-supported silver bismuthate as an efficient electrocatalyst for oxygen reduction reaction in zinc-oxygen batteries. *Electrochim. Acta* **2016**, *197*, 68–76. [CrossRef]

22. Guo, D.; Dou, S.; Li, X.; Xu, J.; Wang, S.; Lai, L.; Liu, H.K.; Ma, J.; Dou, S.X. Hierarchical MnO_2/rGO hybrid nanosheets as an efficient electrocatalyst for the oxygen reduction reaction. *Int. J. Hydrogen Energy* **2016**, *41*, 5260–5268. [CrossRef]

23. Xia, W.; Mahmood, A.; Liang, Z.; Zou, R.; Guo, S. Earth-Abundant Nanomaterials for Oxygen Reduction. *Angew. Chem. Int. Ed.* **2016**, *55*, 2650–2676. [CrossRef] [PubMed]

24. Liang, Y.; Li, Y.; Wang, H.; Zhou, J.; Wang, J.; Regier, T.; Dai, H. Co_3O_4 nanocrystals on graphene as a synergistic catalyst for oxygen reduction reaction. *Nat. Mater.* **2011**, *10*, 780–786. [CrossRef] [PubMed]

25. Hu, F.P.; Zhang, X.G.; Xiao, F.; Zhang, J.L. Oxygen reduction on Ag-MnO_2/SWNT and Ag-MnO_2/AB electrodes. *Carbon* **2005**, *43*, 2931–2936. [CrossRef]

26. Sheng, Z.H.; Gao, H.L.; Bao, W.J.; Wang, F.B.; Xia, X.H. Synthesis of boron doped graphene for oxygen reduction reaction in fuel cells. *J. Mater. Chem.* **2011**, *22*, 390–395. [CrossRef]

27. He, J.; He, Y.; Fan, Y.; Zhang, B.; Du, Y.; Wang, J.; Xu, P. Conjugated polymer-mediated synthesis of nitrogen-doped carbon nanoribbons for oxygen reduction reaction. *Carbon* **2017**, *124*, 630–636. [CrossRef]

28. Pan, J.; Wang, Q.; Sun, Y.; Wang, Z. Analysis of electrochemical mechanism of coprecipitated nano-$Ag_4Bi_2O_5$ as super high charge–discharge rate cathode materials for aqueous rechargeable battery. *Electrochim. Acta* **2012**, *59*, 515–521. [CrossRef]

29. Wang, Q.; Pan, J.; Sun, Y.; Wang, Z. A high capacity cathode material-MnO_2 doped with nano $Ag_4Bi_2O_5$ for alkaline secondary batteries. *J. Power Sources* **2012**, *199*, 355–359. [CrossRef]

30. Goh, F.W.T.; Liu, Z.; Ge, X.; Zong, Y.; Du, G.; Hor, T.S.A. Ag nanoparticle-modified MnO_2 nanorods catalyst for use as an air electrode in zinc-air battery. *Electrochim. Acta* **2013**, *114*, 598–604. [CrossRef]

31. Chen, Y.; Liu, S.; Yu, L.; Liu, Q.; Wang, Y.; Dong, L. Efficient carbon-supported $Ag-MFe_2O_4$ (M = Co, Mn) core–shell catalysts for oxygen reduction reactions in alkaline media. *Int. J. Hydrogen Energy* **2017**, *42*, 11304–11311. [CrossRef]

32. Sun, S.; Miao, H.; Xue, Y.; Wang, Q.; Li, S.; Liu, Z. Oxygen reduction reaction catalysts of manganese oxide decorated by silver nanoparticles for aluminum-air batteries. *Electrochim. Acta* **2016**, *214*, 49–55. [CrossRef]

33. Zuo, L.X.; Jiang, L.P.; Abdel-Halim, E.S.; Zhu, J.J. Sonochemical preparation of stable porous MnO_2 and its application as an efficient electrocatalyst for oxygen reduction reaction. *Ultrason. Sonochem.* **2017**, *35*, 219–225. [CrossRef] [PubMed]

34. Cao, S.; Han, N.; Han, J.; Hu, Y.; Fan, L.; Zhou, C.; Guo, R. Mesoporous Hybrid Shells of Carbonized Polyaniline/Mn_2O_3 as Non-Precious Efficient Oxygen Reduction Reaction Catalyst. *ACS Appl. Mater. Interfaces* **2016**, *8*, 6040–6050. [CrossRef] [PubMed]

35. Lee, K.; Ahmed, M.S.; Jeon, S. Electrochemical deposition of silver on manganese dioxide coated reduced graphene oxide for enhanced oxygen reduction reaction. *J. Power Sources* **2015**, *288*, 261–269. [CrossRef]

36. Zhang, Y.Q.; Tao, H.B.; Liu, J.; Sun, Y.F.; Chen, J.; Hua, B.; Thundat, T.; Luo, J.-L. A rational design for enhanced oxygen reduction: Strongly coupled silver nanoparticles and engineered perovskite nanofibers. *Nano Energy* **2017**, *38*, 392–400. [CrossRef]

37. Guo, S.; Zhang, X.; Zhu, W.; He, K.; Su, D.; Mendoza-Garcia, A.; Ho, S.F.; Lu, G.; Sun, S. Nanocatalyst superior to Pt for oxygen reduction reactions: The case of core/shell Ag(Au)/CuPd nanoparticles. *J. Am. Chem. Soc.* **2014**, *136*, 15026–15033. [CrossRef] [PubMed]